

LA-UR-15-27357 (Accepted Manuscript)

High-resolution In-situ Observations of Electron Precipitation-Causing EMIC Waves

Rodger, C Hendry, A. Cliverd, M Kletzing, C Brundell, j Reeves, Geoffrey D.

Provided by the author(s) and the Los Alamos National Laboratory (0000-00-00).

To be published in: Geophysical Research Letters, Vol.42, Iss.22, p.9633–9641, November 28, 2015.

DOI to publisher's version: 10.1002/2015GL066581

Permalink to record: http://permalink.lanl.gov/object/view?what=info:lanl-repo/lareport/LA-UR-15-27357

Disclaimer

Approved for public release. Los Alamos National Laboratory, an affirmative action/equal opportunity employer, is operated by the Los Alamos National Security, LLC for the National Nuclear Security Administration of the U.S. Department of Energy under contract DE-AC52-06NA25396. Los Alamos National Laboratory strongly supports academic freedom and a researcher's right to publish; as an institution, however, the Laboratory does not endorse the viewpoint of a publication or guarantee its technical correctness.



- High-resolution In-situ Observations of Electron Precipitation-Causing EMIC
- 2 Waves
- 3 Craig J. Rodger and Aaron T. Hendry
- 4 Department of Physics, University of Otago, Dunedin, New Zealand
- 5 Mark A. Clilverd
- 6 British Antarctic Survey (NERC), Cambridge, United Kingdom
- 7 Craig A. Kletzing
- 8 Department of Physics and Astronomy, University of Iowa, Iowa City, Iowa, United States of America
- 9 James B. Brundell
- 10 Department of Physics, University of Otago, Dunedin, New Zealand
- 11 Geoffrey D. Reeves

- 12 Space Science and Application Group, Los Alamos National Lab, Los Alamos, United States of America
- 14 Major Topic or Scientific Question: EMIC waves are thought to be highly important
- drivers of energetic electron loss from the radiation belt, however, there are very few
- 16 experimental examples of precipitation-causing EMIC-events with limited measurements of
- the waves or precipitation.
- 18 New Scientific Knowledge: Here we have, for the first time, simultaneous in-situ
- measurements of the properties of the EMIC wave, the plasma conditions, and the
- precipitation fluxes for a case study event, as well as 4 additional examples of EMIC driven
- 21 precipitation.
- 22 **Broad Implications:** There is increasing evidence of the importance of EMIC waves to
- radiation belt dynamics. However, the lack of experimental quantification of the waves &

precipitation means they are only roughly estimated in radiation belt models. We provide measurements.

- **Main point # 1:** EMIC waves thought to be highly important drivers of electron loss from
- the outer radiation belt.
- 29 Main point # 2: To date there are few experimental examples of precipitation-causing
- 30 EMIC-events.
- Main point # 3: Simultaneous insitu measurements of EMIC wave, plasma, & precipitation
- 32 flux provided for first time.

Abstract. Electromagnetic Ion Cyclotron (EMIC) waves are thought to be important drivers of energetic electron losses from the outer radiation belt through precipitation into the atmosphere. While the theoretical possibility of pitch angle scattering-driven losses from these waves has been recognized for more than 4 decades, there have been limited experimental precipitation observations to support this concept. We have combined satellite-based observations of the characteristics of EMIC waves, with satellite and ground-based observations of the EMIC-induced electron precipitation. In a detailed case study, supplemented by an additional 4 examples, we are able to identify for the first time the location, size, and energy range of EMIC-induced electron precipitation inferred from coincident precipitation data and relate them to the EMIC wave frequency, wave power, and ion-band of the wave as measured in-situ by the Van Allen Probes. These observations will better constrain modeling into the importance of EMIC wave-particle interactions.

1. Introduction

48

It has long been recognized that wave-particle interactions with Electromagnetic Ion 49 Cyclotron (EMIC) waves are an important driver for precipitation of relativistic electrons 50 [e.g., Thorne and Kennel, 1971; Summers and Thorne, 2003; Thorne, 2010]. EMIC waves are 51 observed in the Pc1-Pc2 frequency range (0.1-5 Hz). Unstable ion ring distributions of tens to 52 hundreds of keV ring current ions cause the waves to be generated near the magnetic equator 53 54 propagating as left-handed circularly polarized waves, hence the term "Ion Cyclotron". 55 Recent experimental studies have shown EMIC wave growth can occur at all local times and can persist for hours and sometimes even days [Paulson et al., 2014; Saikin et al., 2015]. 56 Recent modeling studies have concluded that EMIC waves are very important sources of 57 relativistic and ultra-relativistic electron losses from the outer radiation belt [e.g., Drozdov et 58 al., 2015; Ni et al., 2015]. 59 Despite the decades of recognition that EMIC waves could be significant drivers of electron 60 precipitation, until recently there has been little experimental evidence of this. However, 61 some progress is now being made. Some of the earliest confirmation comes from ground-62 based measurements showing evidence of relativistic electron precipitation from 63 subionospheric VLF and riometer observations along with the start of simultaneous EMIC 64 65 waves in ground-based magnetometers [Rodger et al., 2008]. Following on from this the properties of probable EMIC-wave precipitation events detected using the expected signature 66 for EMIC-wave driven losses seen in low-Earth orbit satellite data have been presented 67 [Carson et al., 2012]. One of these probable EMIC-wave precipitation events was investigated in a case study using multiple ground-based experiments [Clilverd et al., 2015], 69 and was confirmed to be intense and EMIC-wave driven, but with unexpectedly low-energy 70 cutoffs <400 keV similar to those suggested by Hendry et al. [2014]. At highly relativistic 71 72 electron energies, indirect evidence of the efficiency of EMIC waves to drive losses has been

provided by Canadian ground-based magnetometer data and >2.3 MeV trapped relativistic 73 electron from the Van Allen probes [Usanova et al., 2014]. Thus, although there is increasing 74 evidence of electron precipitation from EMIC waves, the detailed characteristics of the 75 precipitation and associated waves remain uncertain. 76 However, there are many examples in the literature where EMIC waves are observed on the 77 78 ground or in space for which there appear to be no electron precipitation occurring, even when the measurements are available [e.g., Usanova et al., 2014; Engebretson et al., 2015]. 79 There is also growing recent experimental evidence which suggest that EMIC-waves may 80 precipitate electrons with energies as low as a few hundred keV [Hendry et al., 2014; 81 Clilverd et al., 2015; Blum et al., 2015] rather than the relativistic energies which are widely 82 produced in theoretical modeling [e.g., Meredith et al., 2003; Chen et al., 2011; Usanova et 83 al., 2014]. There is some theoretical support for such comparatively low energy thresholds 84 for EMIC-driven electron precipitation. The minimum resonant energy for a He-band EMIC 85 wave inside the plasmasphere was shown to be as low as ~100 keV for waves at ~1 Hz 86 [Omura and Zhao, Fig.2, 2013] and some quasi-linear theory has indicated minimum 87 resonance energies of ~300-400 keV [Summers and Thorne, 2003; Ukhorskiy et al., 2010]. 88 In order to better constrain modeling and understand the importance of EMIC wave-particle 89 90 interactions it is necessary to have in-situ observations of the wave and plasma characteristics for EMIC waves which are confirmed to be driving electron precipitation. In this paper we 91 provide in-situ observations supported by ground-based precipitation measurements to fulfill 92 this goal. We provide a detailed description of one event, identifying for the first time the 93 location, size, and energy range of EMIC-induced electron precipitation caused by waves 94 with in-situ measurements of EMIC wave frequency, wave power, and ion-band. We also 95 provide the wave and plasma parameters for 4 other similar events. 96

2. Experimental Datasets

2.1 Van Allen Probes Observations

We make use of multiple experiments onboard the Van Allen Probes, in particular the magnetometer and ELF-VLF and LF observations from the Electric and Magnetic Field Instrument Suite and Integrated Science (EMFISIS) [*Kletzing et al.*, 2013], including the cold plasma densities measurements [*Kurth et al.*, 2015]. EMFISIS provides observations of the EMIC waves as well as the geomagnetic field intensities. Pitch-angle resolved electron fluxes are provided by the Magnetic Electron Ion Spectrometer (MagEIS) [*Blake et al.*, 2013] and the Relativistic Electron-Proton Telescope (REPT) [*Baker et al.*, 2013] instruments.

106

107

108

109

110

111

112

113

98

99

100

101

102

103

104

105

2.2 Low Earth Orbit Precipitation Observations

One source of precipitation observations comes from the Medium Energy Proton and Electron Detector (MEPED) instrument onboard the Polar-orbiting Operational Environmental Satellite (POES) [*Evans and Greer*, 2004]. This dataset is unusual in that it measures precipitation electron fluxes inside the bounce loss cone. The characteristics of the POES electron precipitation measurements have been comprehensively described in the literature [e.g., *Rodger et al.*, 2010a,b; *Carson et al.*, 2012].

114

115

116

117

118

119

120

121

122

123

2.3 Ground-based Observations

The other source of precipitation observations comes from narrow band subionospheric very low frequency (VLF) sites that are part of the Antarctic Arctic Radiation-belt dynamic deposition VLF Atmospheric Research Konsortia (AARDDVARK) network [Clilverd et al., 2009; for further information see the description of the www.physics.otago.ac.nz/space/AARDDVARK homepage.htm]. Subionospheric responds to electron precipitation which penetrates beneath the lower boundary of the ionosphere, that is electrons with minimum detectable electron precipitation energies of ~150 keV (day) and ~50 keV (night) [Rodger et al., 2012].

125

126

127

128

129

130

131

132

133

134

135

136

137

138

139

140

141

142

143

144

145

146

147

148

149

3. EMIC Event on 24 September 2013 - Wave Activity

Figure 1 presents a set of spectrograms showing an EMIC event which started at 16:42 UT on 24 September 2013 observed by EMIFISIS onboard RBSP-A. The upper 3 spectrograms are the 3 components of the magnetic field in GSM coordinates. The lower panel of this figure shows the variation in the magnitude of the geomagnetic field, also observed by the EMIFISIS magnetometer. Shortly before the onset of the EMIC wave the geomagnetic field changes, with the magnitude of the total field altering by ~30 nT in 4 minutes from 16:40 UT. This change can also be seen in the He and O ion gyrofrequencies which are plotted as white lines in the spectrogram panels. It is likely that this magnetic field compression triggered the underlying instability that produced the wave, as has been previously observed across a wide range of MLT (see the discussion in Engebretson et al. [2015]). This is a fairly strong and clear example of a He-band EMIC wave event. A summary of the wave and plasma properties determined from the EMFISIS observations of this event are given in Table 1, which shows that this event occurred in the afternoon sector and inside the plasmasphere, although it is likely to have been close to the plasmapause given the electron density value. The upper panel of Figure 2 shows a spectrogram of the EMFISIS magnetic field ELF and VLF observations from RBSP-A across the same time period as shown in Figure 1. Here the spectrograms of the summed magnetic field components have been taken. The lower panel of this figure is the wave-normal angle for the observations shown in the upper panel. Typically, signals with wave normal angles <45° are likely to be whistler mode waves, while those >75° would be indicative of magnetosonic waves [Gurnett and Bhattacharjee, 2005] that are restricted to the region of the geomagnetic equator. Figure 2 indicates that the ELF-VLF wave activity in the time period considered is guiet. Around this time there is a ~100-200 Hz magnetosonic wave that is fading out, as well as a weak ~50-90 Hz magnetosonic wave which starts around the time of the magnetospheric compression.

Whistler mode wave activity is weak, particularly in the time period of the strong EMIC

wave. It is well known that whistler mode waves can pitch angle scatter electrons and cause

precipitation [e.g. *Thorne*, 2010], whereas magnetosonic waves are up to two orders of

magnitude less effective at driving precipitation [*Shprits et al.*, 2013]

4. Precipitation Observations

4.1 AARDDVARK

155

156

157

158

159

160

161

162

163

164

165

166

167

168

169

170

171

172

173

At 16:42 UT the northern hemisphere footprint of the RBSP-A spacecraft was located near Iceland. We have examined AARDDVARK data at this time, concentrating on Atlanticlongitude observations in the region of the RBSP-A observations. The upper two panels of Figure 3 show examples of the AARDDVARK observations made from St John's, Canada (STJ, red line) and Reykjavik, Iceland (REK, blue line). The amplitude and phase perturbations for two transmitters are plotted, with callsign NRK (red line in the Figure, located in Iceland) and NDK (blue line, located in North Dakota, USA). Figure 3 presents the change in amplitude in phase relative to undisturbed conditions, i.e., the change relative to the quiet day curve. There are clear amplitude perturbations starting at 16:42 UT (marked by the dashed vertical line). We observe consistent evidence of subionospheric perturbations beginning at the start time of the RBSP-observed EMIC wave seen in Figure 1. As there is no significant whistler mode wave activity occurring at this time (as shown in Figure 2), the EMIC wave is the most likely candidate for driving the electron precipitation causing the observed AARDDVARK precipitation. The lower panel of Figure 3 shows a geographic map of the AARDDVARK paths analyzed in this study. Note that there is both an AARDDVARK receiver and a VLF transmitter in Iceland, with the NRK transmitter symbol largely obscured. In this plot

AARDDVARK paths which were seen to respond to precipitation at the EMIC wave start time are shown in green, while the unresponsive paths are shown as dashed light blue lines. The AARDDVARK observations are clearly consistent with precipitation occurring near Iceland around the *L*-shells of the RBSP-footprint. The size of the precipitation patch is sufficiently wide enough that transmitter receiver paths to the immediate east and west of Iceland are affected, but not so wide to affect those paths from Western European transmitters to Finland, or from NPM to the Antarctic station, Halley. The observed region of the EMIC-driven precipitation covers ~13-17 MLT.

4.2 POES Observations

Near the start of the period during which the EMIC wave was observed by RBSP-A, there was a serendipitous conjunction with NOAA-15, one of the POES satellites that have been extensively used to investigate radiation belt precipitation. The orbital track of NOAA-15 passed from south to north at the eastern edge of Iceland. At 16:41:55 UT the MEPED instrument onboard this satellite observed a burst of proton and electron precipitation with the signature expected from EMIC waves [Sandanger et al., 2009], detected by an automatic algorithm [Carson et al., 2012]. Such precipitation triggers have recently been shown to be associated with observed EMIC waves [Hendry, A. T., C. J. Rodger, M. A. Clilverd, M. J. Engebretson, M. R. Lessard, I. R. Mann, T. Raita, and D. K. Milling, First large scale survey of POES-detected EMIC wave driven energetic electron precipitation, J. Geophys. Res., (in preparation), 2015.]. The location of this algorithm-trigger event is shown as the blue star in Figure 3, very close to the eastern end of the RBSP-A atmospheric footprint. As this observation was made at essentially the same location and time as the start of the RBSP-A EMIC wave observation, the precipitation includes both protons and a strong relativistic component as expected for effective EMIC-wave scattering, and RBSP-A

reports no significant ELF/VLF wave activity, we assume the POES precipitation event was produced by the observed EMIC wave.

The precipitation spike has been analyzed as described in section 3.2 of *Clilverd et al.* [2015]. By using the proton and electron precipitation measurements and a detailed understanding of the instrument response [*Yando et al.*, 2011], one can determine an energy spectrum, flux magnitude, and energy cutoff estimations for the observed precipitation. This precipitation event is best fit with a power-law, with spectral gradient values from -2.7 to -1.7, lower energy precipitation cutoffs of 140-230 keV, upper cutoff estimates of 1.6-8 MeV, and precipitation magnitudes of ~1.25×10⁴ cm⁻²sr⁻¹s⁻¹.

The location of the POES trigger event and the RBSP-A footprints provide useful

208

209

210

201

202

203

204

205

206

207

4.3 AARDDVARK Modeling

211 constraints on the likely longitudinal range of the precipitation affecting the paths from GQD and DHO to Iceland, i.e., the transmitters to the east of the Reykjavik receiver. We 212 undertake modeling of the subionospheric perturbations predicted from precipitation 213 214 defined by the POES energy and power-law gradient, using approaches previously 215 described [e.g., Rodger et al., 2012; Clilverd et al., 2015]. We find that the modeling is sensitive to the initial conditions, for example comparatively 216 217 small changes in the starting location of the energetic electron precipitation change along the path (i.e., changes of tens of km). This is likely due to the relatively short, all sea path 218 from the transmitter to receiver, such that there is a high number of significant modes 219 220 present in the Earth ionosphere waveguide, and also the small ionospheric region affected. 221 Our modeling of the perturbations observed on the transmissions from DHO 222 $(\Delta Amplitude=+1.8 dB, \Delta Phase=-3^{\circ})$ and GQD $(\Delta Amplitude=+0.6 dB, \Delta Phase=-3^{\circ})$, at the 223 EMIC-wave onset time, indicates these changes are consistent with the effect caused by imposing the POES precipitation observations, i.e. flux magnitudes of ~1×10⁴ cm⁻²sr⁻¹s⁻¹. 224

226

227

228

229

230

231

232

233

234

235

236

237

238

239

240

241

242

243

244

245

246

247

248

249

The modeling reproduces the observations for power law gradients which have low energy cutoffs, i.e. ~200 keV. It was not possible to successfully model the subionospheric VLF perturbations using low energy cutoffs of ~1 MeV. Such cutoffs produce much larger amplitude and phase perturbations than observed. Therefore, the AARDDVARK observations confirm the POES satellite flux and energy cutoffs.

5. Trapped Electron Flux Observations

Figure 4 shows the RBSP-A MagEIS pitch angle resolved trapped fluxes with 1 MeV (upper panel) and 225 keV energies (lower panel). At the time of the magnetospheric compression and the start of the EMIC wave the fluxes change to a butterfly distribution, with s a 50% decrease in the 90° pitch angles fluxes from 16:41-16:44 UT. A similar signature is seen in the MagEIS fluxes at energies >143 keV, and in REPT fluxes ≤2.6 MeV. The REPT fluxes >2.6 MeV are at noise levels. There is no evidence of significantly different behavior between the 2.6 MeV fluxes and those at lower energies, in apparent contradiction to the conclusions of *Usanova et al.* [2014], although this could be obscured by the changes leading to the butterfly distribution. Such butterfly distributions can be produced by magnetopause shadowing or by field line stretching and drift shell splitting [e.g., Roederer et al., 1970; Sibeck et al., 1987]. However, this does not explain the observations in our case, due to the small time dispersion between the energies. The source of the distribution should be only ~ 0.6 MLT away to be consistent with the energy dispersion observed (i.e., located at ~16 MLT). While we note that the butterfly distribution is unlikely to be caused by magnetopause shadowing, there has not been evidence suggesting such pitch angle distributions can be produced by EMIC waves. Nonetheless, the change to this distribution makes it essentially impossible to see evidence of the pitch angle scattering driving the observed precipitation.

6. Additional Events

In our examination of RBSP-A EMIC wave data and comparison with precipitation data we found 4 other events in which RBSP-A observed an EMIC wave, there was little evidence of confounding ELF/VLF whistler-mode wave activity, and AARDDVARK sites at Churchill (Canada), Fairbanks (Alaska), and Sodankylä (Finland) confirmed the presence of energetic electron precipitation. The RBSP-A in-situ measurements of EMIC wave and plasma parameters for these 4 additional events, along with those for 24 September 2013, are given in Table 1. All of these 5 events have butterfly distributions in the MagEIS trapped electron fluxes which begin near the wave start time.

In the current study we have chosen to concentrate on the analysis of the 24 September 2013 event, due to the serendipitous conjunctions between RBSP-A, NOAA-15, and AARDDVARK network observations. None of the other events listed in Table 1 have such close conjunctions. We note that there are multiple POES-triggers on 27 August 2013, and that the events on this day may deserve more attention in a future study.

7. Summary

For the first time we have combined satellite-based observations of the characteristics of EMIC waves, with satellite and ground-based observations of the EMIC-induced electron precipitation. In a detailed case study, supplemented by an additional 4 examples, we are able to identify the location, size, energy range of EMIC-induced electron precipitation inferred from coincident POES/AARDDVARK data and relate them to the EMIC wave frequency, PSD wave power, and ion-band as measured by the Van Allen Probes.

- We find that:
- 1. We find that the precipitation-causing EMIC waves typically occur over the MLT range 16-00 UT, and at $L\sim5.4+/-0.4$. The background plasmaspheric electron densities are ~100 el/cc, suggesting waves that are located close to the plasmapause. The frequency of

274 the EMIC waves are typically 0.3-0.5 Hz, and are mostly found within the helium band. The typical wave power spectral density is $\sim 1 \text{ nT}^2/\text{Hz}$, with peak powers $\sim 10 \text{ times higher}$. 275 276 2. The EMIC-induced electron precipitation was detected by the ground-based 277 AARDDVARK network, with one coincident measurement made by one of the NOAA POES satellites. The region of electron precipitation was small in geomagnetic latitude, i.e., 278 $<50 \text{ km} (\Delta L=0.15)$, but high in flux, i.e., $\sim 10^4 \text{ cm}^{-2} \text{sr}^{-1} \text{s}^{-1}$, with a power law energy spectrum 279 beginning at ~200 keV. Radio wave propagation modeling of the AARDDVARK 280 observations are supportive of the POES detection of a narrow latitudinal precipitation 281 patch, as well as extended in longitude through several hours of MLT, and occurring at the 282 283 time of the EMIC wave observed by RBSP. 284 Acknowledgments. The authors would like to thank Richard Yeo for hosting the 285 AARDDVARK receiver in Reykjavik, the following institutional AARDDVARK hosts: 286 Churchill Northern Studies Center USGS/Magnetic Observatories Fairbanks, and 287 Sodankylä Geophysical Observatory. We would also like to acknowledge the researchers 288 289 and engineers of NOAA's Space Environment Center for the provision of the data and the 290 operation of the SEM-2 instrument carried onboard these spacecraft, the many teams 291 involved in the Van Allen Probes, and the developers of the Autoplot interactive data tool. The research at University of Iowa was supported by JHU/APL contract 921647 under 292 293 NASA prime contract NAS5-01072. Data availability is described at the following websites: http://rbspgway.jhuapl.edu/ (Van 294 Allen **Probes** Science Gateway), http://emfisis.physics.uiowa.edu/ 295 (EMFISIS), 296 http://www.rbsp-ect.lanl.gov/data_pub/rbspa/mageis/level3/_(MagEIS), http://www.rbspect.lanl.gov/data pub/rbspb/rept/level3/ (REPT), http://www.rbsp-297

(MegEphem),

ect.lanl.gov/data_pub/rbspa/MagEphem/def/2013/

- 299 http://satdat.ngdc.noaa.gov/sem/poes/data/ (POES SEM-2),
- http://www.physics.otago.ac.nz/space/AARDDVARK homepage.htm (AARDDVARK).

References

301

- Baker, J. B., et al. (2013), The Relativistic Electron-Proton Telescope (REPT) Instrument on
- Board the Radiation Belt Storm Probes (RBSP) Spacecraft: Characterization of Earth's
- Radiation Belt High-Energy Particle Populations, Space Sci. Rev., 179, 337–381,
- 306 10.1007/s11214-012-9950-9.
- Blake, J. B., et al. (2013), The magnetic electron ion spectrometer (MagEIS) instruments
- aboard the radiation belt storm probes (RBSP) spacecraft, Space Sci. Rev., 179, 383–421,
- 309 doi:10.1007/s11214-013-9991-8.
- Blum, L. W., A. Halford, R. Millan, J. W. Bonnell, J. Goldstein, M. Usanova, M.
- Engebretson, M. Ohnsted, G. Reeves, H. Singer, et al. (2015), Observations of coincident
- EMIC wave activity and duskside energetic electron precipitation on 18–19 January 2013,
- Geophys. Res. Lett., 42, 5727–5735, doi:10.1002/2015GL065245.
- Carson, B. R., C. J. Rodger, and M. A. Clilverd (2012), POES satellite observations of
- EMIC-wave driven relativistic electron precipitation during 1998–2010, J. Geophys. Res.
- 316 Space Physics, 118, 232–243, doi:10.1029/2012JA017998.
- Clilverd, M. A., C. J. Rodger, N. R. Thomson, J. B. Brundell, Th. Ulich, J. Lichtenberger, N.
- Cobbett, A. B. Collier, F. W. Menk, A. Seppälä, P. T. Verronen, and E. Turunen (2009),
- Remote sensing space weather events: the AARDDVARK network, Space Weather, 7,
- 320 S04001, doi:10.1029/2008SW000412.
- Clilverd, M. A., R. Duthie, R. Hardman, A. T. Hendry, C. J. Rodger, T. Raita, M.
- Engebretson, M. R. Lessard, D. Danskin, and D. K. Milling (2015), Electron precipitation
- from EMIC waves: A case study from 31 May 2013. J. Geophys. Res. Space Physics, 120,
- 3618–3631. doi: 10.1002/2015JA021090.
- Drozdov, A. Y., Y. Y. Shprits, K. G. Orlova, A. C. Kellerman, D. A. Subbotin, D. N. Baker,
- H. E. Spence, and G. D. Reeves (2015), Energetic, relativistic, and ultrarelativistic
- 327 electrons: Comparison of long-term VERB code simulations with Van Allen Probes
- measurements. J. Geophys. Res. Space Physics, 120, 3574–3587. doi:
- 329 10.1002/2014JA020637.

- Engebretson, M. J., et al. (2015), Van Allen probes, NOAA, GOES, and ground observations
- of an intense EMIC wave event extending over 12 h in magnetic local time, J. Geophys.
- Res. Space Physics, 120, doi:10.1002/2015JA021227.
- Gurnett, D. A., and A. Bhattacharjee (2005), Introduction to Plasma Physics: With Space and
- Laboratory Applications, Cambridge Univ. Press, New York.
- Hendry, A. T., C. J. Rodger, B. R. Carson, and M. A. Clilverd (2014), Investigating the upper
- and lower energy cutoffs of EMIC-wave driven precipitation events, pp. 4, IEEE Xplore,
- doi: 10.1109/URSIGASS.2014.6929964.
- Hendry, A. T., C. J. Rodger, M. A. Clilverd, M. Engebretson, M. R. Lessard, I. Mann, T.
- Raita, and D. Milling, First large scale survey of POES-detected EMIC wave driven
- energetic electron precipitation, J. Geophys. Res., (in preparation), 2015.
- Kletzing, C. A., et al. (2013), The electric and magnetic field instrument suite and integrated
- studies (EMFISIS) on RBSP, Space Sci. Rev., 179, 127–181.
- Kurth, W. S., De Pascuale, S., Faden, J. B., Kletzing, C. A., Hospodarsky, G. B., Thaller, S.
- and Wygant, J. R. (2015), Electron densities inferred from plasma wave spectra obtained
- by the Waves instrument on Van Allen Probes. J. Geophys. Res. Space Physics, 120: 904–
- 914. doi: 10.1002/2014JA020857.
- Mauk, B. H., N. J. Fox, S. G. Kanekal, R. L. Kessel, D. G. Sibeck, A. Ukhorskiy (2013),
- Science Objectives and Rationale for the Radiation Belt Storm Probes Mission, Space Sci.
- Rev., Vol. 179, 3-27, doi:10.1007/s11214-012-9941-x.
- Meredith, N. P., R. M. Thorne, R. B. Horne, D. Summers, B. J. Fraser, and R. R. Anderson
- 351 (2003), Statistical analysis of relativistic electron energies for cyclotron resonance with
- EMIC waves observed on CRRES, J. Geophys. Res., 108, 1250,
- doi:10.1029/2002JA009700, A6.
- Ni, B., X. Cao, Z. Zou, C. Zhou, X. Gu, J. Bortnik, J. Zhang, S. Fu, Z. Zhao, R. Shi, et al.
- 355 (2015), Resonant scattering of outer zone relativistic electrons by multi-band EMIC waves
- and resultant electron loss timescales, J. Geophys. Res. Space Physics, 120,
- doi:10.1002/2015JA021466.
- Omura, Y., and Q. Zhao (2013), Relativistic electron microbursts due to nonlinear pitch angle
- scattering by EMIC triggered emissions, J. Geophys. Res. Space Physics, 118, 5008–5020,
- 360 doi:10.1002/jgra.50477.
- Paulson, K. W., C. W. Smith, M. R. Lessard, M. J. Engebretson, R. B. Torbert, and C. A.
- Kletzing (2014), In Situ Observations of Pc1 Pearl Pulsations by the Van Allen Probes,
- Geophys. Res. Lett., 41, doi:10.1002/2013GL059187.

- Roederer, J. G. (1970), Dynamics of Geomagnetically Trapped Radiation, Springer, New
- 365 York.
- Rodger, C. J., B. R. Carson, S. A. Cummer, R. J. Gamble, M. A. Clilverd, J-A. Sauvaud, M.
- Parrot, J. C. Green, and J.-J. Berthelier (2010b), Contrasting the efficiency of radiation
- belt losses caused by ducted and non-ducted whistler mode waves from ground-based
- transmitters, J. Geophys. Res., 115, A12208, doi:10.1029/2010JA015880.
- Rodger, C. J., M. A. Clilverd, A. J. Kavanagh, C. E. J. Watt, P. T. Verronen, and T. Raita
- (2012), Contrasting the responses of three different ground-based instruments to energetic
- electron precipitation, Radio Sci., 47, RS2021, doi:10.1029/2011RS004971.
- Rodger, C. J., M. A. Clilverd, J. C. Green, and M. M. Lam (2010a), Use of POES SEM-2
- observations to examine radiation belt dynamics and energetic electron precipitation into
- the atmosphere, J. Geophys. Res., 115, A04202, doi: 10.1029/2008JA014023.
- Rodger, C. J., T. Raita, M. A. Clilverd, A. Seppälä, S. Dietrich, N. R. Thomson, and T. Ulich
- 377 (2008), Observations of relativistic electron precipitation from the radiation belts driven
- by EMIC waves, Geophys. Res. Lett., 35, L16106, doi:10.1029/2008GL034804.
- Saikin, A. A., J.-C. Zhang, R. C. Allen, C. W. Smith, L. M. Kistler, H. E. Spence, R. B.
- Torbert, C. A. Kletzing, and V. K. Jordanova (2015), The occurrence and wave properties
- of H+-, He+-, and O+-band EMIC waves observed by the Van Allen Probes, J. Geophys.
- Res. Space Physics, 120, doi:10.1002/2015JA021358.
- Sandanger, M., F. Søraas, M. Sørbø, K. Aarsnes, K. Oksavik, and D. Evans (2009),
- Relativistic electron losses related to EMIC waves during CIR and CME storms, Journal
- of Atmospheric and Solar-Terrestrial Physics, 71 (10-11), 1126 1144,
- doi:10.1016/j.jastp.2008.07.006.
- Shprits Y. Y., A. Runov, and B. Ni (2013), Gyro-resonant scattering of radiation belt
- electrons during the solar minimum by fast magnetosonic waves, J. Geophys. Res. Space
- Physics, 118, 648–652, doi:10.1002/jgra.50108.
- Sibeck, D. G., R. W. McEntire, A. T. Y. Lui, R. E. Lopez, and S. M. Krimigis (1987),
- Magnetic field drift shell splitting: Cause of unusual dayside particle pitch angle
- distributions during storms and substorms, J. Geophys. Res., 92(A12), 13485–13497,
- doi:10.1029/JA092iA12p13485.
- Summers, D., and R. M. Thorne (2003), Relativistic electron pitch-angle scattering by
- electromagnetic ion cyclotron waves during geomagnetic storms, J. Geophys. Res., 108,
- 396 1143, doi:10.1029/2002JA009489, A4.

- Thorne, R. M. (2010), Radiation belt dynamics: The importance of wave-particle interactions,
- 398 Geophys. Res. Lett., 37, L22107, doi:10.1029/2010GL044990.
- Thorne, R. M., and C. F. Kennel (1971), Relativistic electron precipitation during magnetic
- storm main phase, J. Geophys. Res., 76, 4446, doi:10.1029/JA076i019p04446.
- Ukhorskiy, A. Y., Y. Y. Shprits, B. J. Anderson, K. Takahashi, and R. M. Thorne (2010),
- Rapid scattering of radiation belt electrons by storm-time EMIC waves, Geophys. Res.
- 403 Lett., 37, L09101, doi:10.1029/2010GL042906.
- Usanova, M. E., et al. (2014), Effect of EMIC waves on relativistic and ultrarelativistic
- electron populations: Groundbased and Van Allen Probes observations, Geophys. Res.
- 406 Lett., 41, doi:10.1002/2013GL059024.
- 407 Yando, K., R. M. Millan, J. C. Green, and D. S. Evans (2011), A Monte Carlo simulation of
- the NOAA POES Medium Energy Proton and Electron Detector instrument, J. Geophys.
- 409 Res., 116, A10231, doi:10.1029/2011JA016671.
- 410 ____
- M. A. Clilverd, British Antarctic Survey (NERC), High Cross, Madingley Road,
- Cambridge CB3 0ET, England, U.K. (e-mail: macl@bas.ac.uk).
- J. B. Brundell, A. T. Hendry and C. J. Rodger, Department of Physics, University of Otago,
- 414 P.O. Box 56, Dunedin, New Zealand. (email: james@brundell.co.nz,
- aaron.hendry@otago.ac.nz, crodger@physics.otago.ac.nz).
- 416 C. A. Kletzing, Department of Physics and Astronomy, University of Iowa, Iowa City,
- Iowa, U.S.A. (email: craig-kletzing@uiowa.edu)
- Geoffrey D. Reeves, Space Science and Application Group, Los Alamos National Lab,
- Los Alamos, U.S.A. (email: reeves@lanl.gov)
- 420
- 421 RODGER ET AL.: EMIC WAVES DRIVING PRECIPITATION
- 422
- 423

Date	24-Sep-13	24-Mar-13	14-Aug-13	27-Aug-13	27-Aug-13
Time (UT)	16:41	6:57	4:57	15:52	16:52
L	5.1	5.7	5.3	5.3	5.8
MLT	16.5	23.7	18.1	17.9	18.7
f_{upper} (Hz)	0.5	0.9	0.2	0.55	0.35
f_{lower} (Hz)	0.25	0.3	0.4	0.47	0.15
PSD wave power					
typical (nT ² /Hz)	0.8	0.1	3	0.3	0.3
peak (nT ² /Hz)	10	1	42	2	6
N_e (cm ⁻³)	190	79	63	112	43
f_{pe} (kHz)	120	80	72	95	58
f_{ce} (kHz)	5.5	3.9	4.3	4.9	3.1
RBSP satellite	Α	В	В	A	A
Ion Band	Не	Н	Не	Не	Не

Table 1. Properties at the times of the observed EMIC wave driven precipitation events. The first event is that described in detail in this study. The parameters listed are as measured by RBSP-A. f_{upper} , f_{lower} : upper and lower EMIC wave frequency, PSD: EMIC wave power spectral density, N_e : cold electron density, f_{pe} : electron plasma frequency, f_{ce} : electron gyrofrequency.

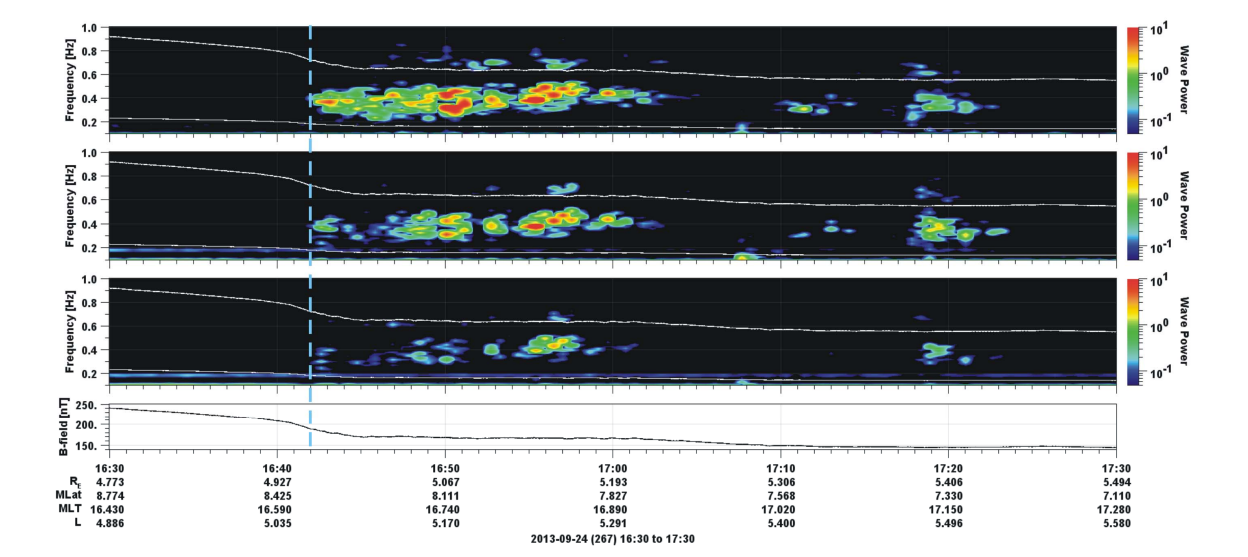


Figure 1. The three upper panels show spectrograms of the 3 components of the magnetic field in GSM coordinates from the EMFISIS experiment onboard RBSP-A on 24 September 2013. Wave power has units of nT²/Hz. The white lines show the local ion gyrofrequencies for He (upper) and oxygen (lower) ions. The lowest panel presents the absolute value of the DC magnetic field reported by the same instrument. A blue dashed line marks the start of the EMIC-wave at 16:42 UT.

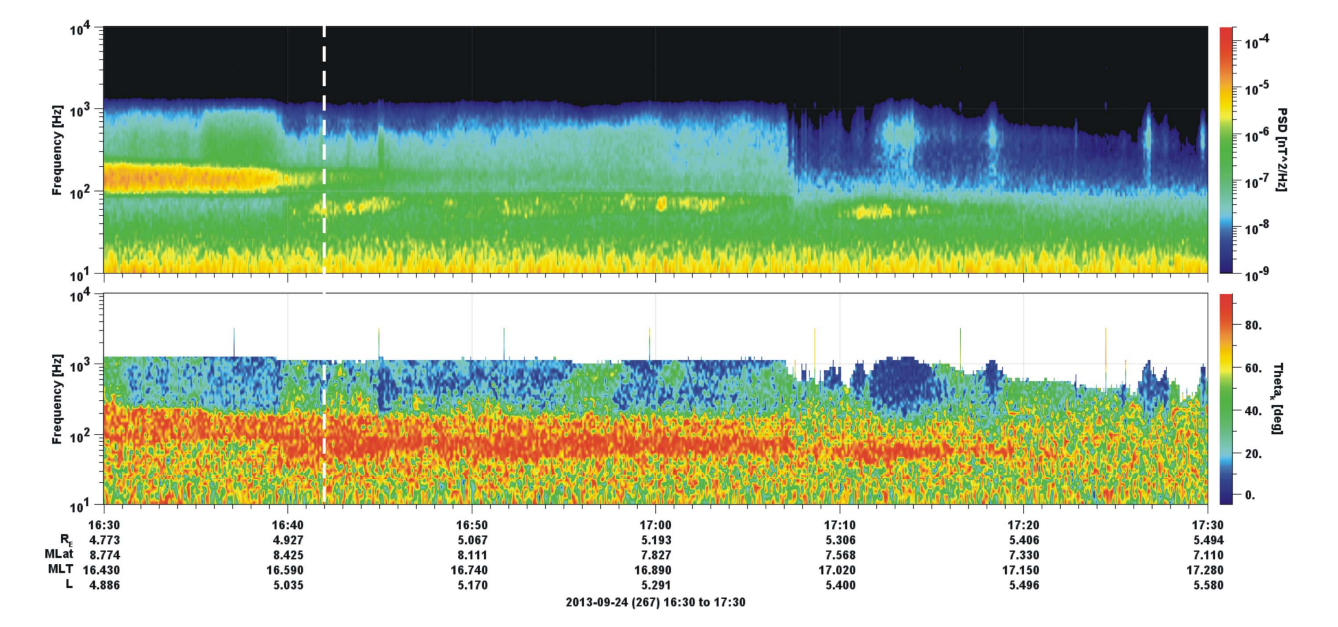


Figure 2. EMFISIS ELF/VLF magnetic field observations for the same time period shown in Figure 1. The upper panel is the spectrogram of the summed magnetic field components with units of nT²/Hz. The lower panel shows the wave-normal angle with units of degrees, determined from the upper panel waveforms.

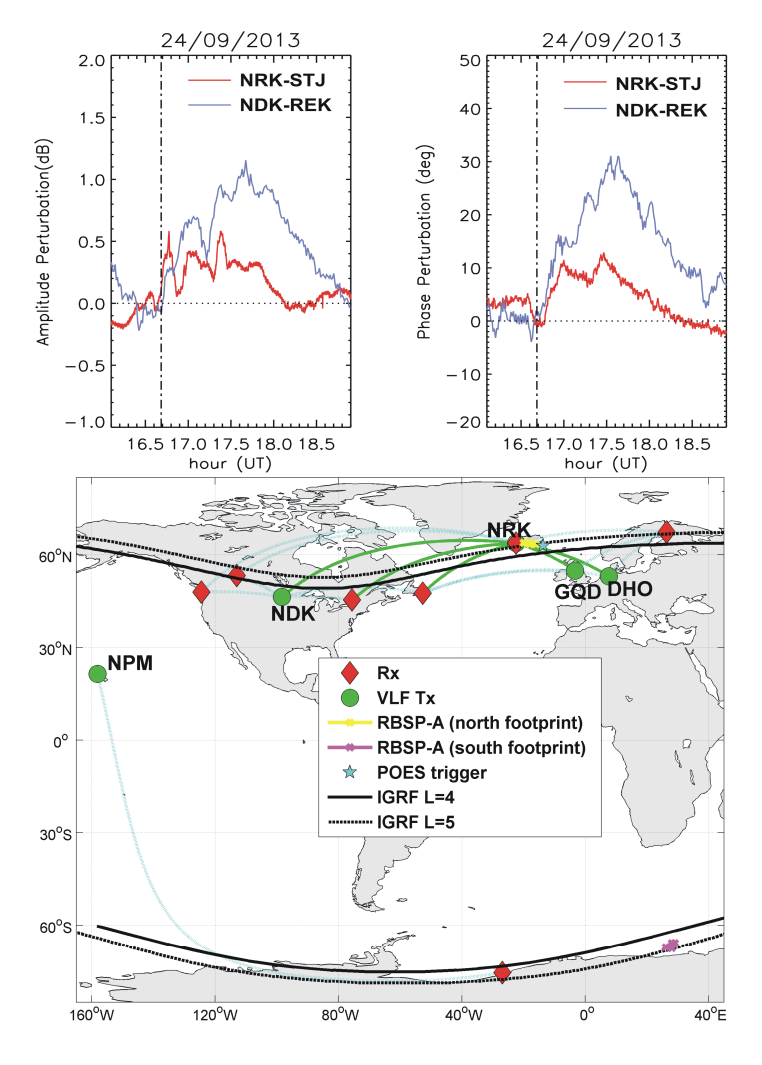


Figure 3. Summary of AARDDVARK observations at the event time. The upper panels shows amplitude and phase perturbations observed on the path NRK-St John's (Canada) (STJ, red) and NDK-Reykjavík (REK, blue). The black dashed line marks 16:42 UT. The lower panel is a map of the AARDDVARK paths analyzed in this study. RBSP-A northern (yellow) and southern (magenta) footprints are shown, as is the POES trigger sub-satellite point (blue star), AARDDVARK receivers (red diamonds), and VLF transmitters (green circles). In this plot AARDDVARK paths which were seen to respond to precipitation at the EMIC wave start time are shown in green, while the unresponsive paths are shown as dashed light blue lines.

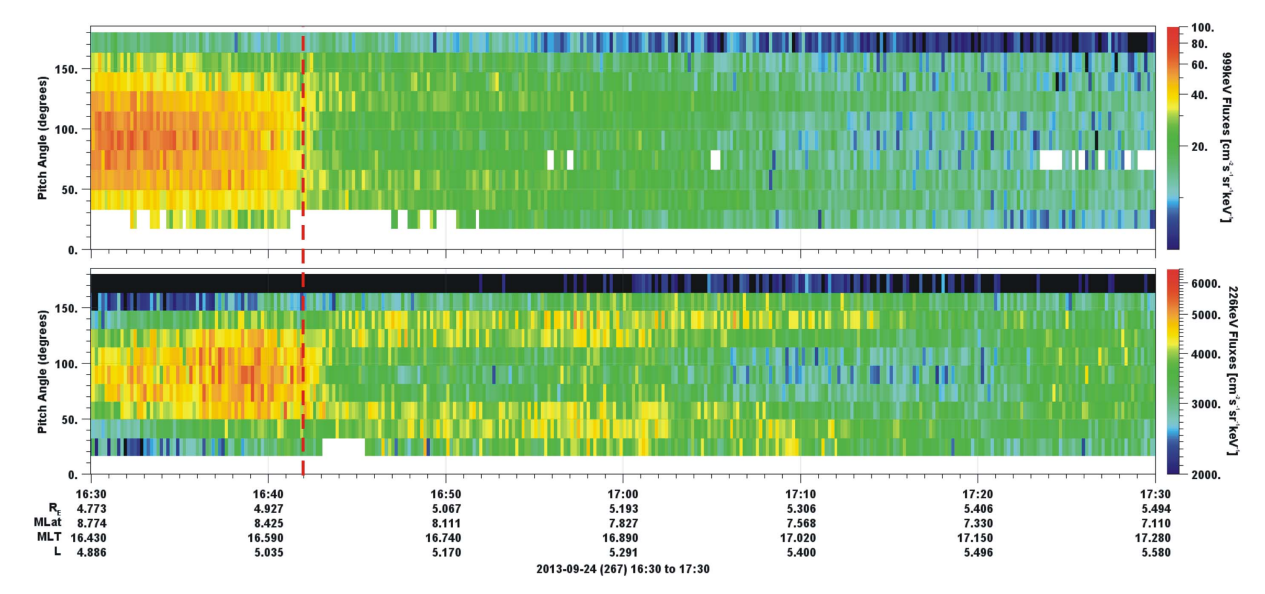


Figure 4. Butterfly pitch angle distributions seen in the MagEIS 1 MeV flux distributions (upper panel) and the 225 keV distributions (lower panel). The dashed red line marks the start of the EMIC wave seen in Figure 1.